Comparison of MHD Simulations of the Solar Wind with In-Situ Measured Plasma and Magnetic Field Parameters at 1 AU

Corinna Gressl, Kanzelhöhe Observatory-IGAM, Institute of Physics, University of Graz, Austria

1 Introduction and Motivation

Solar wind models are an important tool for space weather forecasting. Today the best approach for simulations of the heliosphere is to use coupled models: A coronal model simulating the phenomena in the corona (up to typically $20-30$ $R_\odot$) is coupled with a model simulating the propagation of solar wind parameters through the heliosphere (Odstrčil et al., 2008).

ENLIL is a time-dependent 3D MHD model of the heliosphere that is able to simulate the structure and evolution of characteristic solar wind parameters like density, speed, temperature, and magnetic field. ENLIL is suited for simulations of the inner and middle heliosphere and can be used to model the background solar wind as well as to simulate transient disturbances in the heliosphere, so-called ENLIL-with-cone-model (Odstrčil et al., 2002; Odstrčil, 2003). ENLIL can be coupled with one of two coronal models: Wang-Sheeley-Arge (WSA) or Magnetohydrodynamics Around Sphere (MAS). The MAS model is a 3-D numerical model for simulations of the corona (Riley et al., 2001), WSA is an empirical model developed to forecast accurate SW conditions at 1 AU by using an empirical relationship between the solar wind speed and the magnetic flux tube expansion rate (Wang and Sheeley, 1990; Arge and Pizzo, 2000). MAS and WSA use synoptic maps of the Sun's line-of-sight magnetic field observed in the photosphere. The coronal models provide the inner boundary conditions for the ENLIL code which then simulates the propagation of solar wind structures outward into the heliosphere up to 10 AU.

For validating the performance of solar wind models, the model results have to be compared to in-situ measurements of the solar wind. A previous study by Lee et al. (2009) gave a comparison of modeled and measured solar wind parameters for Carrington rotations (CR) 1999 to 2038 with a time resolution of 3.6 hours. The solar wind parameters were derived at fixed values for distance (1 AU) and latitude (0°) from ENLIL/WSA and ENLIL/MAS model output, not taking into account spatial variatons due to the spacecraft's orbit. Lee et al. (2009) found a general good agreement for large scale structures and for time scales of several days.

We aimed to study the performance of the solar wind models ENLIL/MAS and ENLIL/WSA at time scales smaller than 1 day and at the exact spacecraft position (L_1). Therefore we extracted the solar wind parameters from the ENLIL model output at the spacecraft position, taking into account variations in spacecraft coordinates over the course of a CR. We requested model runs at CCMC at the highest possible resolution, resulting in a time resolution of 1.8 hours. For testing of the solar wind models we compared the parameters

proton density, solar wind speed, temperature, and radial and total magnetic field strength to in-situ measurements from Wind and ACE. For the comparison we chose the year 2005 as a time period with low solar activity.

2 Data

2.1 ENLIL Model Runs

To run simulations of the heliosphere we requested ENLIL model runs at the CCMC homepage. We used the ENLIL model for simulations of the background solar wind with inner boundary conditions from WSA and MAS with the aim to produce a stationary solar wind solution.

For the Carrington Rotations 2025 – 2037 three different model runs per CR were performed:

- ENLIL/MAS (with magnetograms from National Solar Observatory (NSO)),
- ENLIL/WSA with magnetograms from NSO,
- ENLIL/WSA with magnetograms from Mount Wilson Observatory (MWO).

For the simulations a grid resolution of $1024 \times 120 \times 360$ covering 1024 pixels in radial distance r, 120 in latitude θ ($\pm 60°$) and 360 in longitude ϕ ($0° - 360°$) with an outer boundary of 2 AU was chosen.

Due to bad magnetograms some of the models could not be run. For the time period of CR 2028 – 2032 (25^{th} of March to 8^{th} of August 2005) the results for all three different model runs are available. Thus, in our study we particularly focus on this time range during 2005.

CCMC provided the results of the simulations online with quick look graphics and visualization tools. ASCII files can be downloaded for model results at Earth, at Mars, at Mercury, at Messenger, and at Venus. On special request the full simulation data available as netCDF files were provided. The usage of netCDF files allows high flexibility when choosing the exact location for which the simulation results are needed. The netCDF files contain the data of the model results up to $\pm$ 59.5° in latitude out to the outer boundary of about 2 AU. This makes it possible to extract the solar wind parameters exactly at the position of ACE and Wind as well as for any other position inside the boundaries.

2.2 In-Situ Data

For the comparison with the ENLIL simulations we used the in-situ data from the spacecrafts Wind (Solar Wind Experiment, Ogilvie et al. (1995)) and ACE (SWEPAM, MAG, McComas et al. (1998); Smith et al. (1998)). Both satellites are positioned at Lagrangian Point L_1 and are equipped with instruments to measure the solar wind plasma and magnetic field parameters.

3 Methods

3.1 Extracting Data from netCDF Files

The ENLIL netCDF output files contain the data of the stationary solar wind solution for the whole simulation grid with 1024×120×360 (x1 × x2 × x3) cells with a resolution of 1° in latitude and longitude (corresponding to a time resolution of 1.8 hours). Figure 1 illustrates the ENLIL simulation cells in the stationary model output. The x1-cells refer to the distance to the Sun, for ENLIL/MAS starting at 0.141 AU (30.3 $R_\odot$) and for ENLIL/WSA starting at 0.101 AU (21.7 $R_\odot$). The 120 x2-cells range from 59.5° north to 59.5° south in heliocentric Earth equatorial coordinates (HEEQ). The 360 x3-cells refer to the heliographic longitude with a resolution of 1°.

For the comparison with in-situ measurements, graphs for the time evolution of solar wind parameters during one CR are needed. For producing the graphs the data from the netCDF files were extracted along the x3-cells as shown in Figure 1: the extraction along the x3-cells is illustrated by an orange arrow.

The x-axis for the graph is gained by converting the heliographic longitude into time: Due to the rotation of the Sun the radially outward moving solar wind appears structured along the Parker spiral for a coordinate system fixed at the Sun. Thus, the Earth revolves through the stationary solar wind solution in the course of one synodical rotation of the Sun (27.2753 days; in Figure 1 the route of the Earth along the x3-cells is indicated by an orange arrow). The 360 x3-cells that represent the heliographic longitude with a resolution of 1° thus correspond to the time of one full CR with 27.27 days. Therefore the Earth's route along the x3-cells can be used to produce a time axis with a resolution of about 1.8 hours.

Extracting Parameters at Variable Latitude and Distance

The coordinates of ACE and Wind (HEEQ coordinates) shows variations of as much as up to 3° in latitude during the time period of one CR. Near the ecliptic plane, variations of 1° may cause considerable differences in the heliospheric conditions. The distance to the Sun is also variable (due to the elliptic orbit of the Earth and the spacecraft) but it does not impact the results as much as the variations in latitude.

To take into account the variations in distance and latitude that occur during 27.27 days an advanced method for extracting data was developed: the matching x1- and x2-cells were not only calculated for the beginning of the CR but for all 360 data points separately. The spacecraft coordinates were read in for each data point (x3-cells/time axis) and transformed into HEEQ coordinates. Then the nearest x1- and x2-cell to the spacecraft's coordinates were calculated for all 360 x3-cells separately. The data were extracted along the x3-cells, each at the best matching x1-, and x2-cell. The IDL procedure for the extraction was programmed to allow the option to carry out extractions for the position of Earth, ACE, or Wind.

3.2 Data Analysis

For comparing the simulation results obtained from the models ENLIL/WSA and ENLIL/MAS with the observed solar wind parameters at 1 AU we used the following methods:

- linear correlation coefficients to quantify the agreement between the modeled and measured SW parameters,
- cross-correlation analysis to derive the time lag between modeled and measured arrival times of solar wind structures,
- histograms to analyze the distribution of the modeled and observed solar wind parameters.

4 Results

Figure 2 shows the model results of ENLIL/MAS and ENLIL/WSA together with in-situ measurements from Wind and ACE for CR 2028 as an example for a CR with good model results. The maximum speeds of the high speed streams in CR 2028 was simulated well by both models. For the high speed stream arriving (rise of speed in the in-situ data) on the 11^{th} of April 2012 the models differ in absolut timing by about 1 day. The arrival time simulated by ENLIL/MAS is too late, the arrival time simulated by ENLIL/WSA is too early. ENLIL/MAS gives too high peaks for the high density regions at stream interfaces, ENLIL/WSA on the other hand underestimates the density in the high density regions. Both models give too small values for the proton temperature. Also the modeled magnetic field strengths are generally too low. However, peaks in the magnetic field strength that appear after the polarity reversals of the interplanetary magnetic field are simulated well.

We used histograms to analyze the distribution of simulated and measured solar wind parameters. Figure 3 shows the histograms for the parameters density, speed, temperature, and magnetic field strength for CR 2028 – 2032. The histograms show that the simulated solar wind parameters have a different distribution than the parameters measured by Wind. The distributions of modeled solar wind parameters show a much narrower range than the measured ones. ENLIL/WSA reproduces a more realistic distribution of solar wind parameters than ENLIL/MAS.

To quantify the agreement of ENLIL/MAS and ENLIL/WSA with in-situ measurements we calculated correlation coefficients for the single model runs (1 CR = 27.27 days). In addition, the correlation coefficients were calculated for the whole time period CR 2028 – 2032 (24^{th} of March – 8^{th} of August 2005). Figure 4 shows the correlation plots between the model results and the in-situ measurements for all the solar wind parameters under study. The correlation is best for the parameters speed and radial magnetic field strength. For the ENLIL/MAS model runs the correlation coefficients are consistently larger than for the ENLIL/WSA model runs.

To quantify the time lag between the predicted and measured arrival time of solar wind structures we carried out cross-correlations for the different solar wind parameters. In Figure 5 the results for the parameter solar wind speed are shown. The top panel shows the measured and the modeled solar wind speed from 24^{th} of March to 8^{th} of August 2005. The bottom panel gives the results for the cross correlation over this time period. For ENLIL/MAS the time lag is +15 hours (predicted arrival times are too late compared to observations), for the ENLIL/WSA model runs the time lags are −27 and −31 hours (predicted arrival times are too early). The calculated correlation coefficients and the time lags for all solar wind parameters are presented in Figure 6.

Studying several CRs in 2005 we found that by trend the best model results are obtained for the parameter solar wind speed. Also the magnetic sectors of the interplanetary magnetic field are well reproduced by both models. However, the modeled magnetic field strength is lower than in the in-situ measurements. Both models give systematically too low proton temperature at 1 AU. The simulated temperature is too low by about an order of magnitude as compared to observations. The predicted arrival time of solar wind structures is 1 – 1.5 days too early or too late. ENLIL/WSA produces systematically too early arrival times of solar wind structures ($\sim$ 1.5 days). For ENLIL/MAS the predicted arrival times are mostly too late ($\sim$ 1 day).

5 Discussion and Conclusion

The results we gained from comparing ENLIL/MAS and ENLIL/WSA with in-situ measurements from ACE and Wind are in general agreement with the findings of Lee et al. (2009). We found that the model predictions are best for the solar wind parameters proton speed and radial magnetic field strength with correlation coefficients of $\sim 0.3 - 0.5$. The parameter with the least accurate simulation results is the proton temperature that gives systematically too low values. The ENLIL code works with pre-installed scaling factors that cannot be modified by the user requesting runs at CCMC. This could be a possible explanation for the offset in the proton temperatures.

The distribution of the modeled solar wind parameters is different to the distribution of observed parameters. For all parameters the variability of the modeled solar wind parameters is smaller than the measured ones. To avoid numerical problems the models use limits for the simulated solar wind parameters, which could explain the smaller variability of the model results compared to observations. The maximum speeds of high speed streams are well reproduced in the models. However, the total timing of arriving high speed streams is not accurate. The arrival times differ from the in-situ measured arrival times typically by ± 1 to 1.5 days. For the CRs under study we find that ENLIL/MAS produces positive time shifts (i. e. the predicted arrival time is too late) and ENLIL/WSA produces negative time shifts (i. e. the predicted arrival time is too early).

Heliospheric modeling is a complex matter and inaccuracies in the model results can have a wide range of causes. The input to the model runs are synoptic magnetograms, which combine magnetograms of the photosphere over the time of one CR. The spatial resolution of the used magnetograms does not allow to account for spatially small regions of open

field lines. When using the largest simulation grid with $1024 \times 120 \times 360$ cells the time resolution of the ENLIL model results is 1.8 hours. It has to be considered that enlarging the simulation grid does not necessarily lead to a higher time resolution as the effective time resolution is limited by the longitudinal resolution of the input magnetogram (Jian et al., 2011).

Solar activity can worsen the accuracy of the model performance in two ways: First, high CME activity as well as interacting CMEs disturb the interplanetary background solar wind structure. In this case, the effects of CMEs on the solar wind conditions are observed by the in-situ measurements but do not appear in the predictions. Second, the input magnetograms basically give an average of the photospheric magnetic field over the course of one CR. High solar activity, i. e. evolving sunspots or flare or CME eruptions, imply large changes in the solar magnetic field within one CR, that are not captured in the synoptic maps.

We come to the following conclusions:

- ENLIL/MAS and ENLIL/WSA produce the best simulation results for the solar wind parameters proton speed and radial magnetic field strength.
- Both models predict temperatures at 1 AU that are systematically too small by almost an order of magnitude.
- ENLIL/MAS gives a slightly better overall agreement with in-situ measurements at 1 AU than ENLIL/WSA, expressed in better correlation coefficients. However, ENLIL/WSA produces a more realistic distribution of solar wind parameters than ENLIL/MAS.
- The accuracy of ENLIL/WSA and ENLIL/MAS to simulate arrival times of high speed streams is in the range of about ± 1 to 1.5 days. For ENLIL/WSA the simulated high speed streams tend to arrive too early, for ENLIL/MAS too late.

References

C. N. Arge and V. J. Pizzo. "Improvement in the prediction of solar wind conditions using near-real time solar magnetic field updates". J. Geophys. Res.105 (2000) 10465–10480. [ADS].

L. K. Jian, C. T. Russell, J. G. Luhmann, P. J. MacNeice, D. Odstrcil, P. Riley, J. A. Linker, R. M. Skoug, et al. "Comparison of Observations at ACE and Ulysses with Enlil Model Results: Stream Interaction Regions During Carrington Rotations 2016 - 2018". Sol. Phys.273 (2011) 179–203. [ADS].

C. O. Lee, J. G. Luhmann, D. Odstrcil, P. J. MacNeice, I. de Pater, P. Riley, and C. N. Arge. "The Solar Wind at 1 AU During the Declining Phase of Solar Cycle 23: Comparison of 3D Numerical Model Results with Observations". Sol. Phys.254 (2009) 155–183. [ADS].

D. J. McComas, S. J. Bame, P. Barker, W. C. Feldman, J. L. Phillips, P. Riley, and J. W. Griffee. "Solar Wind Electron Proton Alpha Monitor (SWEPAM) for the Advanced Composition Explorer". Space Sci. Rev.86 (1998) 563–612. [ADS].

D. Odstrčil. "Modeling 3-D solar wind structure". Advances in Space Research 32 (2003) 497–506. [ADS].

D. Odstrčil, J. A. Linker, R. Lionello, Z. Mikic, P. Riley, V. J. Pizzo, and J. G. Luhmann. "Merging of coronal and heliospheric numerical two-dimensional MHD models". Journal of Geophysical Research (Space Physics) 107 (2002) 1493. [ADS].

D. Odstrčil, V. J. Pizzo, C. N. Arge, M. M. Bissi, P. P. Hick, B. V. Jackson, S. A. Ledvina, J. G. Luhmann, et al. "Numerical Simulations of Solar Wind Disturbances by Coupled Models". In N. V. Pogorelov, E. Audit, & G. P. Zank, ed., *Numerical Modeling of Space Plasma Flows*, vol. 385 of *Astronomical Society of the Pacific Conference Series*, 167–+ (2008). [ADS].

K. W. Ogilvie, D. J. Chornay, R. J. Fritzenreiter, F. Hunsaker, J. Keller, J. Lobell, G. Miller, J. D. Scudder, et al. "SWE, A Comprehensive Plasma Instrument for the Wind Spacecraft". Space Sci. Rev.71 (1995) 55–77. [ADS].

P. Riley, J. A. Linker, and Z. Mikić. "An empirically-driven global MHD model of the solar corona and inner heliosphere". J. Geophys. Res.106 (2001) 15889–15902. [ADS].

C. W. Smith, J. L'Heureux, N. F. Ness, M. H. Acuña, L. F. Burlaga, and J. Scheifele. "The ACE Magnetic Fields Experiment". Space Sci. Rev.86 (1998) 613–632. [ADS].

Y. Wang and N. R. Sheeley, Jr. "Solar wind speed and coronal flux-tube expansion". Astrophysical Journal355 (1990) 726–732. [ADS].

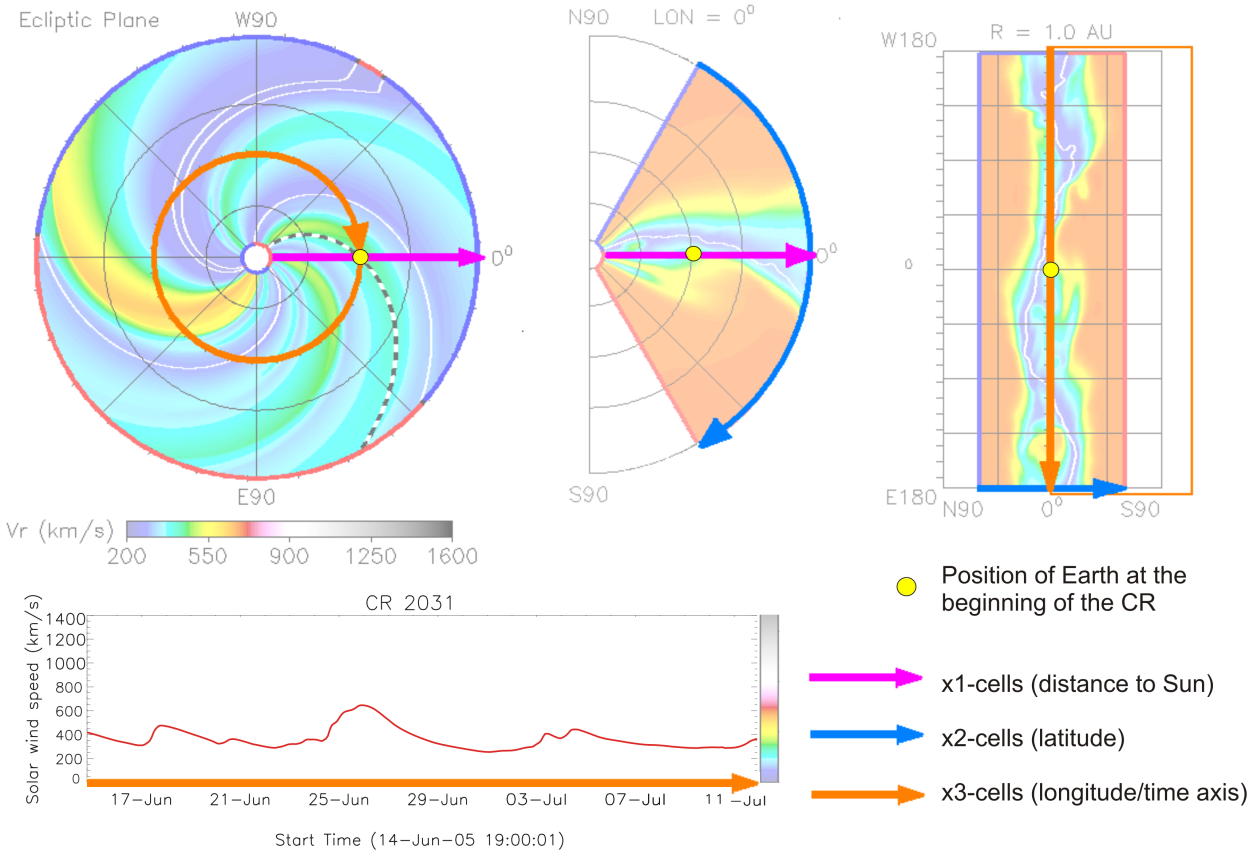

Figure 1: Quick look plot for the ENLIL/MAS simulation of CR 2031 for solar wind parameter proton speed (Source: CCMC/NASA). The colored arrows show the direction of the ENLIL x1-, x2-, and x3-cells. The position of the Earth at the beginning of the CR is marked with a yellow dot. Top left panel: Stationary solar wind solution (speed) for the ecliptic plane (fixed latitude) out to a distance of 2 AU. During the time of one CR the Earth passes through the heliosphere along the orange circle. Middle panel: Proton speed for the heliospheric slice at 0° longitude simulated up to latitudes of ±60° (fixed longitude). Top right panel: Solar wind speed at 1 AU (fixed distance to the Sun). The Earth passes through the stationary solar wind solution along the orange arrow. Bottom panel: Plot for ENLIL/MAS model output as extracted from the netCDF file. The x-axis was produced by converting the heliographic longitude (x3-cells) into time according to the Carrington solar rotation rate of 27.2753 days.

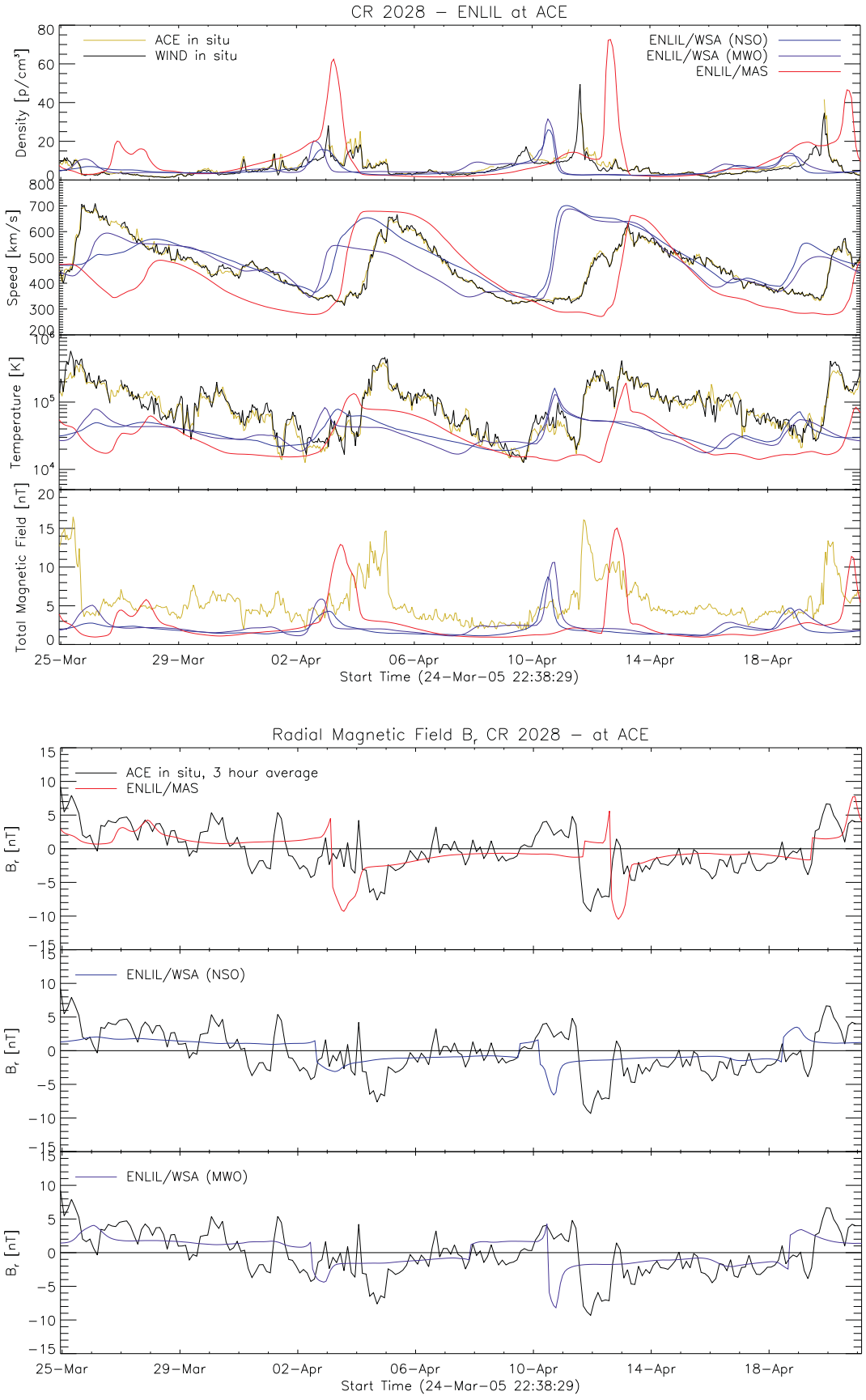

Figure 2: ENLIL/MAS and ENLIL/WSA model results together with in-situ measurements from Wind and ACE for the solar wind parameters density, speed, temperature, total magnetic field strength, and radial magnetic field strength for CR 2028.

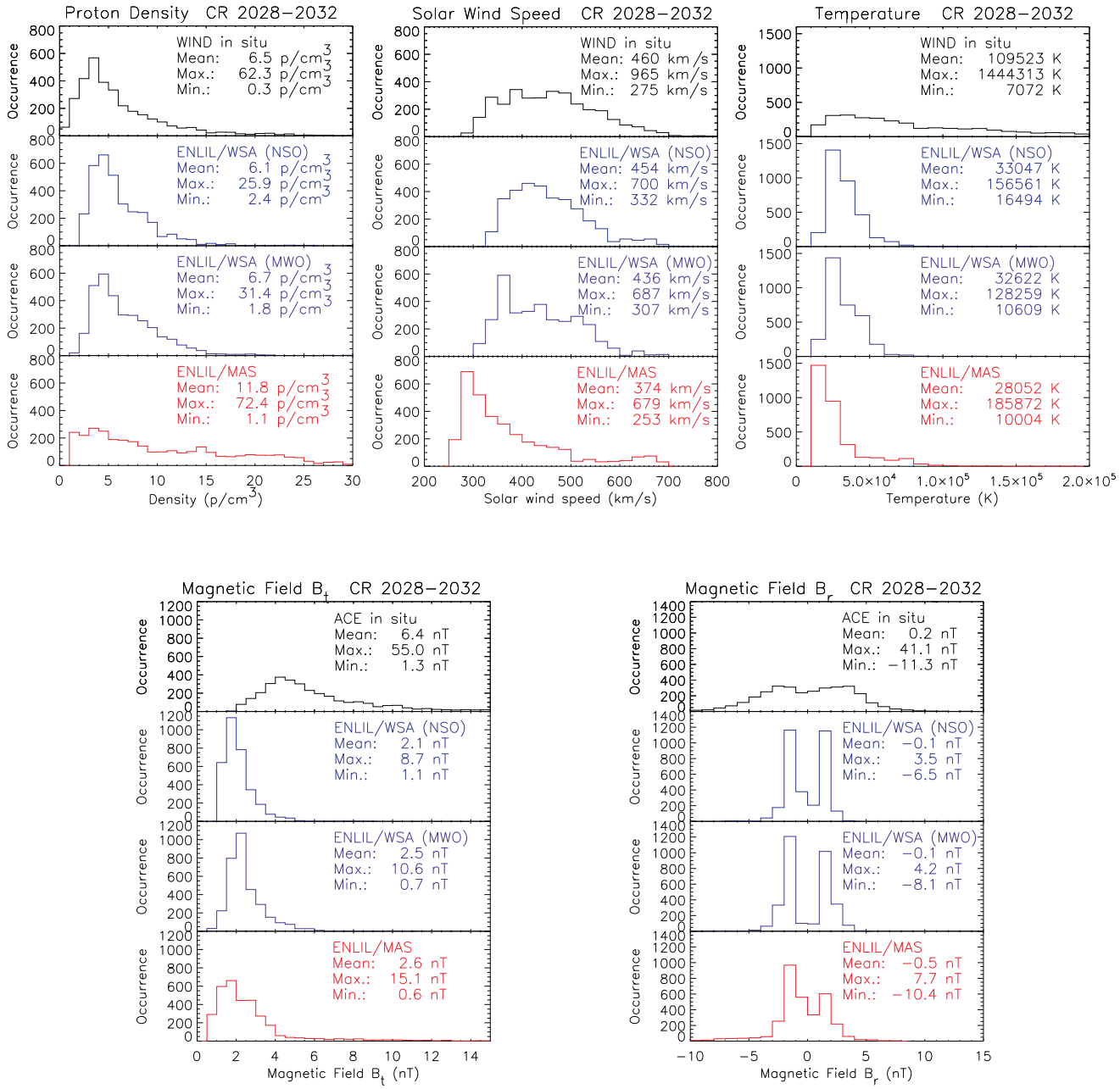

Figure 3: Histograms for solar wind proton density (binsize: 1 p/cm^3), speed (binsize: 25 km/s), temperature (binsize: 10^4 K), total magnetic field (binsize: 0.5 nT) and radial magnetic field (binsize: 1 nT) for CRs 2028 – 2032 (altogether 3265 data points). The top panels show the histograms for the Wind and ACE data, the other three panels show the histograms for ENLIL/MAS and ENLIL/WSA. The maximum, minimum, and average density are displayed on the top right of each histogram.

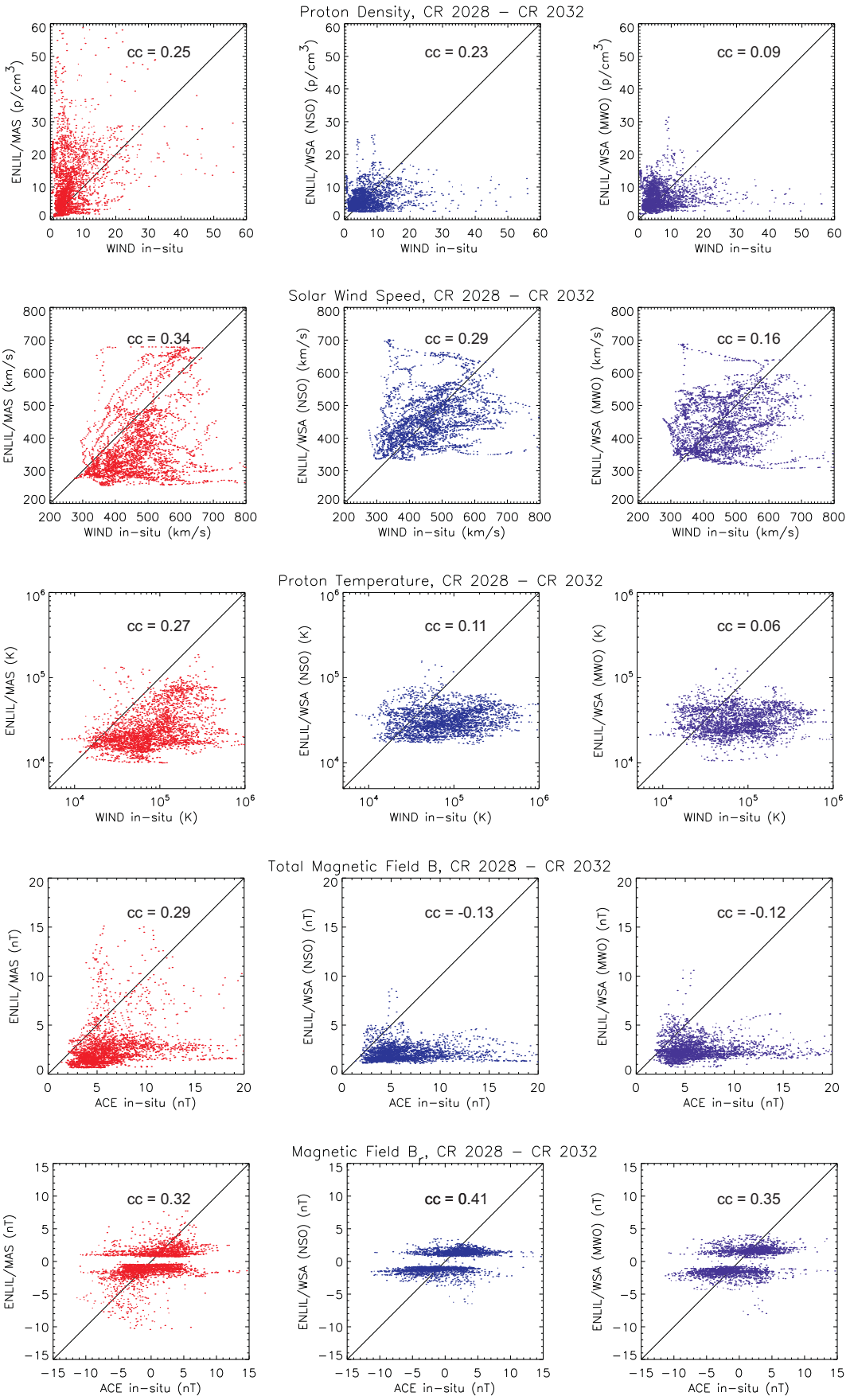

Figure 4: Correlation plots between modeled and measured solar wind parameters for CR 2028 – 2032.

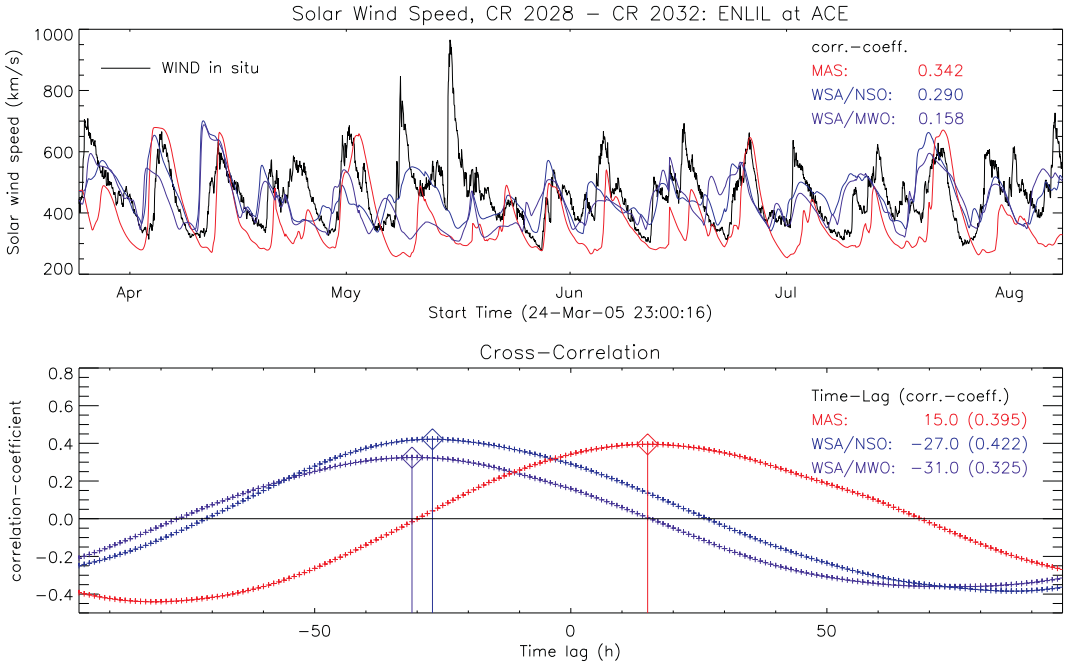

Figure 5: Top panel: Wind solar wind speed for the time period CR 2028 – 2032. Bottom panel: Results for the cross-correlation between ENLIL models and Wind measurements over the whole time period.

CR 2028	**MAS**		**WSA/NSO**		**WSA/MWO**	
	Corr.-Coeff.	*Lag (h)*	*Corr.-Coeff.*	*Lag (h)*	*Corr.-Coeff.*	*Lag (h)*
density	0,293	23	0,194	- 25	0,150	- 26
speed	0,520	- 4	0,371	- 28	0,397	- 30
temp.	0,329	- 1	0,069	- 33	0,115	- 34
B_{total}	0,296	19	-0,030	- 34	-0,057	- 29
B_{radial}	0,335	24	0,367	- 31	0,402	- 26

CR 2028 - 2032	**MAS**		**WSA/NSO**		**WSA/MWO**	
	Corr.-Coeff.	*Lag (h)*	*Corr.-Coeff.*	*Lag (h)*	*Corr.-Coeff.*	*Lag (h)*
density	0,252	25	0,226	- 26	0,091	- 24
speed	0,342	15	0,290	- 27	0,158	- 31
temp.	0,274	4	0,111	- 38	0,058	- 38
B_{total}	0,200	3	-0,007	- 47	0,022	- 66
B_{radial}	0,321	24	0,411	2	0,354	- 24

Figure 6: Correlation coefficients for solar wind parameters and the time shift of the best correlation derived by carrying out cross-correlations for CR 2028 (left panel) and the time period CR 2028 – 2032 (right panel).